Semilocalization transition driven by a single asymmetrical tunneling

P. Wang, K. L. Zhang, and Z. Song*
School of Physics, Nankai University, Tianjin 300071, China

(Received 13 September 2019; revised manuscript received 22 December 2019; accepted 14 January 2020; published 21 February 2020)

A quantum phase transition (QPT) in Hermitian systems is independent of the boundary condition in the thermodynamic limit. However, it may happen for a non-Hermitian system, that the QPT strongly depends on the boundary condition. We investigate the many-body ground-state property of a one-dimensional tight-binding ring with an embedded single asymmetrical dimer based on exact solutions. We employ a semilocalization state to describe a quantum phase that is a crossover from extended to localized state. The peculiar feature is that the decay length is of the order of the system size rather than fixed as a usual localized state. In addition, the spectral statistics is nonanalytic as asymmetrical hopping strengths vary, resulting a sudden charge of the ground state. The distinguishing feature of such a QPT is that the density of the ground-state energy varies smoothly due to unbroken symmetry. However, there are other observables, such as the ground-state center of mass and average current, which exhibit the behavior of second-order QPT. This behavior stems from time-reversal symmetry breaking of a macroscopic number of single-particle eigenstates.

DOI: 10.1103/PhysRevA.101.022111

I. INTRODUCTION

Understanding quantum phase transitions (QPTs) is of central significance to both condensed-matter physics and quantum information science. QPTs occur only at zero temperature due to the competition between different parameters describing the interactions of the system. A quantitative characterization of a QPT is that a certain quantity, such as an order parameter or Chern number, undergoes qualitative changes when some parameters pass through quantum critical points. So far almost all the investigations about QPT focus on systems with translational symmetry, in aid of which the local order parameter and topological invariant can be well defined. In both cases, the ground-state property is encoded in complete set of single-particle eigenstates, forming a Bogoliubov quasiparticle band or Bloch band. A conventional symmetry-breaking QPT concerns all the single-particle eigenstates independently, regardless of the connection between them, while a topological QPT captures global features of the symmetry-respecting single-particle eigenstate sets. There are two prototypical exactly solvable models—the transverse-field Ising model [1] and the Qi-Wu-Zhang model [2]—based on which the concepts and characteristics of conventional and topological QPTs can be well demonstrated. In general, the order parameters and topological index are based on the translational symmetry, which also indicates that the QPT is driven by a global parameter such as external field or uniform coupling constant.

Intuitively, translational symmetry is not necessary for the onset of a QPT; a material in practice usually has an open boundary condition. Theoretically, within the Hermitian regime, a local parameter that controls the boundary usually strongly affects only a few single-particle energy levels and thus cannot affect the onset of a QPT, or any macroscopic quantum phenomena in a many-body system. This contradiction disappears when an infinite system is considered, where the translational symmetry still remains in the bulk. A fundamental question is whether all kinds of QPTs are independent of boundary conditions, including a non-Hermitian system. It is well known that a non-Hermitian system may make many things possible, including a quantum phase transition that induces in a finite system [3–22] unidirectional propagation and anomalous transport [6,23–30], invisible defects [31–33], coherent absorption [34] and self-sustained emission [35–39], loss-induced revival of lasing [40], as well as laser-mode selection [41–43]. Such kinds of novel phenomena can be traced to the existence of an exceptional point, which is a transition point of symmetry breaking for a pair of energy levels. Exploring the novel quantum phase or QPT [44–60] in non-Hermitian systems becomes an attractive topic. And topological features in non-Hermitian fermionic systems have attracted extensive studies [61–66]. Motivated by the recent development of non-Hermitian quantum mechanics [67], both in theoretical and experimental aspects [26,28,67–78], in this paper we investigate the QPTs in the non-Hermitian regime. The purpose of the present work is to present a simple non-Hermitian model to demonstrate alternative types of QPTs which are driven by a local parameter. We study a phenomenon that we dub semilocalization, which is induced by a single asymmetrical tunneling embedded in a uniform tight-binding ring. A semilocalization state is a crossover from extended to localized states, possessing a truncated exponential decay probability distribution. The peculiar feature is that the decay length is of the order of the size of the system rather than fixed as a usual localized state. The single-particle solution of the model shows that the spectral statistics, such as the number and distribution of the complex energy levels,

*songtc@nankai.edu.cn

is controlled by the asymmetrical hopping strength. The eigenstate is a semilocalized state for a complex level while an extended state for a real level. Particularly, a real (complex)-level wave function possesses symmetric (asymmetric) probability distributions and steady (nonsteady) with zero (nonzero) current due to the unbroken (broken) time-reversal symmetry. Although the system is non-Hermitian with a complex single-particle spectrum, the many-body ground-state energy is always real due to the protection of time-reversal symmetry. It exhibits a unconventional QPT arising from the sudden changes of the single-particle spectral statistics: the density of many-body ground-state energy is analytic, while the center of mass and average staggered current of the ground state, as macroscopic quantities, are nonanalytic functions of the asymmetric hopping strength. Accordingly, the transition from a fully real to complex spectrum is associated with the transition from extension to semilocalization.

This paper is organized as follows. In Sec. II we present a non-Hermitian time-reversal symmetric model with asymmetric dimer and the Bethe ansatz solution. In Sec. III, we provide the phase diagram by analyzing the properties of eigenstates with real and complex energy levels, such as the proportion of complex level, the ground-state center of mass, and the ground-state average staggered current. In Sec. IV, we demonstrate the characteristics of second-order QPT. Finally, we give a summary in Sec. V.

II. MODEL AND SOLUTION

Considering a simple uniform tight-binding ring, it is well known that the spectrum is cosine type and cannot be changed largely by a local impurity in general. An additional Hermitian hopping term or even non-Hermitian local on-site complex potential can only alter several energy levels, introducing localized states. However, we will see that another type of non-Hermitian impurity may have an affect on macroscopic energy levels, which plays the key role in the present work.

The Hamiltonian has the form

$$H=\sum_{j=1}^{N-1}c_j^\dagger c_{j+1}+\text{H.c.}+\mu c_N^\dagger c_1+\nu c_1^\dagger c_N, \tag{1}$$

with odd $N/2$, where c_j is the annihilation operator of the fermion at site j. It depicts a uniform tight-binding ring with only a non-Hermitian impurity embedded. A schematic illustration of the model is presented in Fig. 1(a). The non-Hermiticity arises from an asymmetric tunneling between sites 1 and N, represented by hopping strength μ and ν (in this paper, we consider only the case with $\mu,\ \nu>0$ for simplicity). This model is investigated in the previous work [79] in the special case with $\mu\nu=1$. It has been shown that an asymmetric dimer can be realized by the combination of imaginary potential and magnetic flux [80]. Experiments on the asymmetric dimer have been proposed [63,81,82], and an experimental realization of the non-Hermitian Hamiltonian for fermionic systems is also discussed in Ref. [55].

Unlike the usual many-body non-Hermitian tight-binding model, the Hamiltonian H does not have parity-time symmetry and translational symmetry. Owing to the reality of the coupling μ and ν, it possesses time reversal symmetry, i.e.,

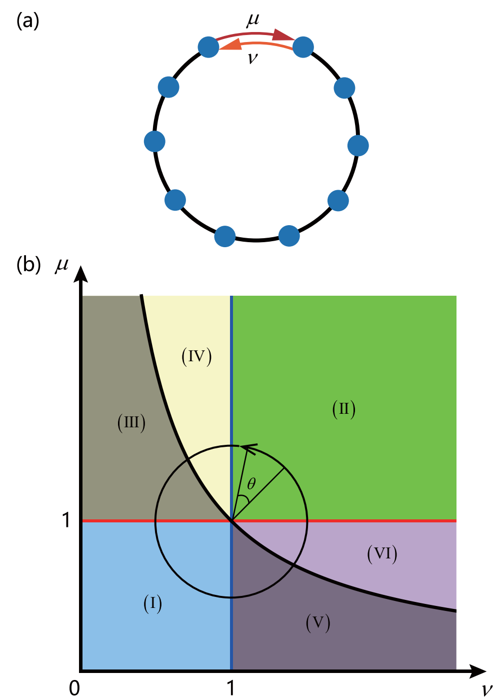

FIG. 1. (a) Schematic of the model, which depicts a uniform tight-binding ring with unitary hopping strength, embedded by a single non-Hermitian dimer. It is an asymmetric tunneling with hopping strength μ and ν. (b) Phase diagram of the system, which is consisted of six regions. In regions (I) and (II), the system has a full real spectrum, while in (III), (IV), (V), and (VI) the spectra are mixed with real and complex energy levels. At curve $\mu\nu=1$, all the energy levels are complex. The inset circle is described by parameter equations $\nu=1+r\cos(\theta)$; $\mu=1+r\sin(\theta)$ goes through all six regions and will be used in the following figures.

$[\mathcal{T},H]=0$, where $\mathcal{T}$ is an antiunitary operator with action $\mathcal{T}^{-1}i\mathcal{T}=-i$. Fortunately, the solution of H can be exactly obtained by the Bethe ansatz technique (see Appendix).

The Hamiltonian can be diagonalized as the form

$$H=\sum_{n=1}^{N}\varepsilon_n\overline{\gamma}_n\gamma_n, \tag{2}$$

where the fermion operators $\overline{\gamma}_n$ and γ_n have the form

$$\overline{\gamma}_n=\sum_{l=1}^{N}f_n^l c_l^\dagger,\ \gamma_n=\sum_{l=1}^{N}\overline{f_n^l}c_l \tag{3}$$

and satisfy the canonical commutative relation

$$\{\gamma_m,\overline{\gamma}_n\}=\delta_{mn}.$$

Here the canonical conjugate operator can be constructed by the relation

$$\overline{f_n^l}(\mu,\nu)=\left[f_n^l(\nu,\mu)\right]^*, \tag{4}$$

and the explicit expression of the wave function is

$$f_n^l=\frac{1}{\sqrt{\Omega}}\sin\left(k_n l+\alpha_n\right),\quad (2<l<N-1)$$

$$f_n^1=\frac{1}{\sqrt{\Omega}},\quad f_n^N=\frac{e^{-ik_n}-\mu e^{ik_n(N-1)}}{\nu-e^{ik_nN}}f_1, \tag{5}$$

where α_n is obtained by $\tan\alpha_n = c_n/s_n$, and

$$s_n = \nu^2 + 1 - \nu\cos(k_nN) + \nu\cos[k_n(N+2)] - p_n\cos k_n, \tag{6}$$

$$c_n = \nu\sin(k_nN) - \nu\sin[k_n(N+2)] + p_n\sin k_n, \tag{7}$$

$$p_n = \cos[k_n(N+1)] - \mu\nu\cos[k_n(N-1)] + (\mu+\nu)\cos k_n. \tag{8}$$

The coefficient Ω_n is determined by the biorthonormal inner product. In the rest of the paper we focus on the Dirac probability, since it can be measured directly in experiments. Then we take the Dirac normalization factor which is obtained from $\sum_{l=1}^{N}|f_n^l|^2 = 1$. The single-particle spectrum has the form

$$\varepsilon_n = e^{ik_n} + e^{-ik_n}, \tag{9}$$

where k_n can be real and complex. The quasi–wave vector k_n for $1 \leqslant n \leqslant N$ has the form

$$k_n = \frac{2n\pi}{N} + \theta_n, \tag{10}$$

where θ_n is determined by the transcendental equation (see Appendix). The transcendental equation is reduced to

$$\tan\theta_n = \frac{(1-\mu\nu)\sin(\theta_nN)}{\mu+\nu-(1+\mu\nu)\cos(\theta_nN)}, \tag{11}$$

for $n = N$ or $N/2$, and

$$\sin(\phi_n + \theta_nN) = \frac{(\mu+\nu)\sin\frac{n\pi}{N}}{\sqrt{1+\mu^2\nu^2-2\mu\nu\cos\frac{2n\pi}{N}}}$$
$$\tan\phi_n = \frac{1+\mu\nu}{1-\mu\nu}\tan\frac{n\pi}{N} \tag{12}$$

otherwise. Obviously, the reality of k_n ($1 \leqslant n \leqslant N$) depends on the values of μ and ν, which will be discussed in detail in the next section.

III. PHASE DIAGRAM

In this section, we analyze the property of the solution and the corresponding implications. At first, we determine the phase diagram from the perspective of spectral statistics, which is characterized by the proportion of the complex levels. Second, we introduce a concept, the semilocalized state, to describe the feature of the eigenstates of complex energy levels. Furthermore, we reveal another exclusive property of the complex-level eigenstates, the nonsteady state, which can be seen only from an evolved (nonequilibrium) state in a Hermitian system.

A. Spectral statistics

According to the solutions obtained in the Appendix, the reality of energy levels obeys the following rules: (i) For $\mu,\nu > 1$, or $\mu,\nu < 1$, all the quasi–wave vectors k_n are either real or imaginary, corresponding to real energy levels. All the eigenstates are nondegenerate except the trivial case with $\mu = \nu = 1$, which reduces the system to be a uniform Hermitian ring. We denote the (nondegenerate) real-energy single-particle eigenstate as $|\psi_{\rm R}^n\rangle$, barring the energy levels $n = N$ and $N/2$. (ii) For $\mu > 1 > \nu$, or $\mu < 1 < \nu$, some complex quasi–wave vectors k_n appear, corresponding to complex energy levels which come in pairs with conjugate eigenenergy. We denote the complex-energy single-particle eigenstate as $|\psi_{\pm}^n\rangle$. (iii) Among them, especially in the case of $\mu\nu = 1$, all k_n becomes complex. Obviously, as one of the characteristics of the spectral statistics, the proportion of the complex level is defined as a function of μ and ν,

$$g(\mu,\nu) = \frac{N_{\rm C}(\mu,\nu)}{N}, \tag{13}$$

which is the ratio of the number of complex levels $N_{\rm C}$ to the total number of levels. In the large-N limit, we have

$$g(\mu,\nu) = \begin{cases} 0, & \mu,\nu \geqslant 1, \text{ or } \mu,\nu \leqslant 1 \\ (\pi - 2k_c)/\pi, & \mu > 1 > \nu, \text{ or } \mu < 1 < \nu, \\ 1, & \mu\nu = 1 \end{cases} \tag{14}$$

where $k_c = |\arcsin[(1-\mu\nu)/(\nu-\mu)]|$ is the critical wave vector separating the real and complex levels. A schematic of the three kinds of regions, which will be shown as a phase diagram, is plotted in Fig. 1(b). To demonstrate the properties of the ratio, 3D profiles of $g(\mu,\nu)$ and the corresponding energy-level structure are plotted in Figs. 2(a)–2(c) and Fig. 3. In Fig. 2(d), we plot the ratios as a function of $\theta \in [0,\pi]$ for a system with finite size N. It indicates that $g(\mu,\nu)$ has many nonanalytic points for small N, and there are only three nonanalytic points on the circle across the lines $\mu = 1$, $\nu = 1$, and $\mu\nu = 1$ in the thermodynamic limit. We will show that such curves are phase boundaries for many-body ground states due to the sudden change of the spectral statistics.

B. Semilocalized state

Unlike a linear operator such as parity, the time-reversal operator $\mathcal{T}$ is an antilinear operator. The $\mathcal{T}$ symmetry breaking is always associated with the appearance of complex levels. The exact solution in the Appendix shows that the single-particle eigenfunction can always be expressed to obey the relations

$$\mathcal{T}|\psi_{\rm R}^n\rangle = |\psi_{\rm R}^n\rangle,\ \mathcal{T}|\psi_{\pm}^n\rangle = |\psi_{\mp}^n\rangle. \tag{15}$$

Owing to the value of k_n, there are three types of wave functions: extended, localized, and semilocalized states. Here the last one is exclusive for non-Hermitian systems. Unlike the localized one, the imaginary part of k_n of semilocalized states θ_n is inversely proportional to N, leading to an incomplete decay distribution (with a truncated tail). Nevertheless, it still supports an imbalanced probability distribution as a crossover from extended to localized states. We employ the center of mass (CoM), which is the expectation value of the CoM operator

$$r_{\rm c} = \frac{1}{N}\sum_{l=1}^{N} l c_l^{\dagger}c_l. \tag{16}$$

Straightforward derivation shows that (i) $\langle r_{\rm c}\rangle \approx 1/2$ for an extended state; (ii) $\langle r_{\rm c}\rangle \approx 0$ (1) for a localized state at the

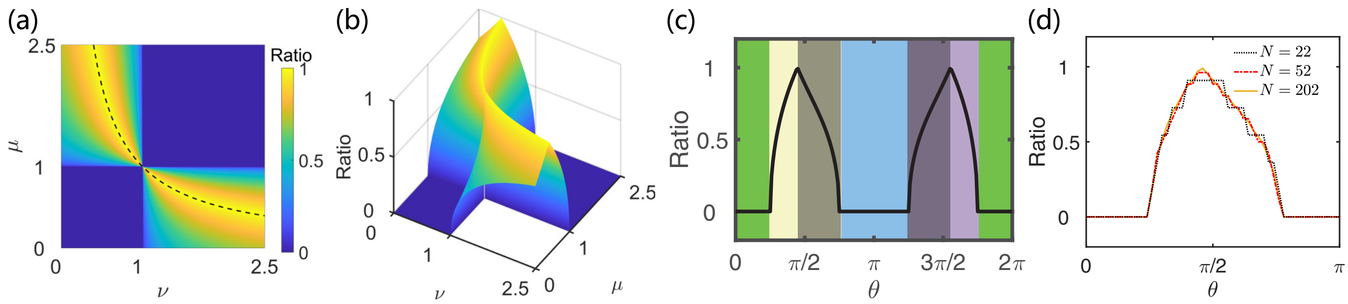

FIG. 2. Plots of the ratio $g(\mu, \nu)$ in $\nu\mu$ plane from Eq. (14) as one perspective of the spectral statistics. (a) Color contour plot. The dished lines indicate the curve $\nu\mu = 1$. The nonanalytic behavior of $g(\mu, \nu)$ at lines $\mu\nu = 1$ are obvious. (b) 3D plot. The nonanalytic behavior of $g(\mu, \nu)$ at curve $\mu\nu = 1$ is highlighted. (c) Plots of the ratio at the loop $\nu = 1 + 0.5\cos(\theta)$; $\mu = 1 + 0.5\sin(\theta)$. The nonanalytic behaviors at the phase boundaries are clearly indicated by the sharp peaks and right-angle turns. (d) Plots of the ratio obtained from numerical diagonalization for systems with finite N. The curves are steplike functions and become smooth as N increases. However, three points across the boundaries $\mu = 1$, $\nu = 1$, and $\mu\nu = 1$ remain nonanalytic.

case $\nu > \mu$ ($\mu > \nu$); and (iii) for a semilocalized state $\langle r_c \rangle$ is a number ranging from 0 to 1. Here we give an example:

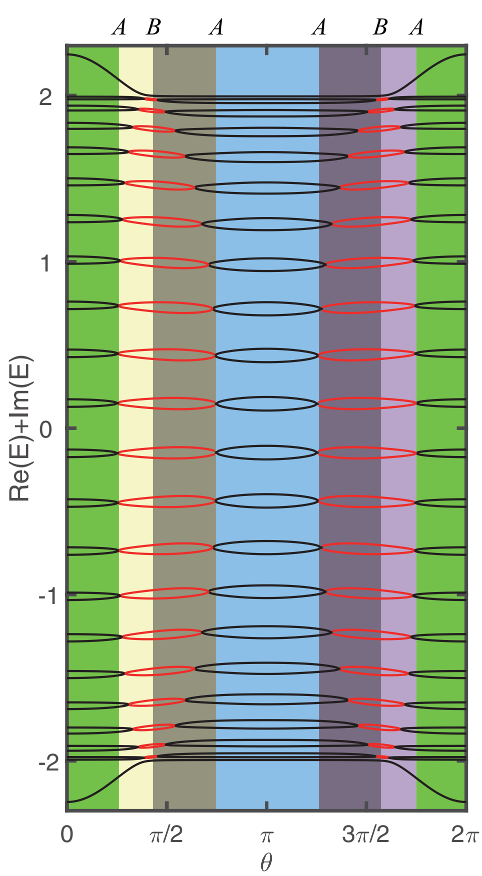

FIG. 3. Plots of energy-level structures for understanding the connection between the spectral statistics and QPTs. Energy levels for the system on the loop $\nu = 1 + 0.9\cos(\theta)$; $\mu = 1 + 0.9\sin(\theta)$ are plotted. Black and red lines represent the real and complex energy levels, respectively. There are two types of QPTs with the boundaries indicated by A and B, respectively. We see that the A-type boundary always corresponds to the appearance of complex levels, while the B -type boundary is located at the maximal number of complex levels. The size of the system is $N = 42$.

when $\mu\nu = 1$ and $\nu > 1 > \mu$, we have

$$\langle r_c \rangle \approx \frac{1}{(\sqrt[N]{\nu^2} - 1)N} + \frac{1}{1 - \nu^2}, \tag{17}$$

in the large-N limit. It is easy to check that $\lim_{\nu\to 1} \langle r_c \rangle = 1/2$, which accords with the above analysis. To demonstrate the above conclusions, profiles of such three types of states and the corresponding $\langle r_c \rangle$ are plotted in Fig. 4(a). We can see that the difference among the three types of eigenstates is obvious.

C. Nonsteady eigenstate

We note that the $\mathcal{T}$-symmetry breaking of $|\psi_{\pm}^{n}\rangle$ indicates that $|\psi_{\pm}^{n}\rangle$ can have nonzero local current, which is defined as

$$J_l = -i\langle (c_l^{\dagger} c_{l+1} - \text{H.c.})\rangle_n, \tag{18}$$

at the position l. Here $\langle ...\rangle_n$ denotes the expectation value for an eigenstate of n level. It is usual that for a Hermitian system, for instance, taking $\mu = \nu = 1$, each eigenstate with nonzero momentum has zero local current. Remarkably, an intriguing feature is that $|\psi_{\pm}^{n}\rangle$ is a nonsteady state, since J_l is position dependent, violating the conservation of current. A nonsteady state can exist in a Hermitian system, such as a moving wave packet in a tight-binding ring. However, it cannot be an eigenstate of a Hermitian system. If $\mu \leftrightarrows \nu$, the current changes the sign. In Fig. 4(b), profiles of the current distributions for three types of eigenstates are plotted.

As a temporary summary, we can conclude that a semilocalized eigenstate has a distinguishing feature from an extended one (the localized eigenstate can be negligible, since there are only two such eigenstates at most): it is a nonsteady state, possessing current and a decay distribution with a size-dependent decay length. Although we refer it to as a "semilocalized state," it exhibits the characteristic of an extended state since it has zero inverse participation ratio (IPR) in the thermodynamic limit. These features should result in a macroscopic property for a many-body ground state.

IV. PHASE TRANSITION

Now we consider the many-body effect of the single-particle spectral statistics. We focus on the ground state for

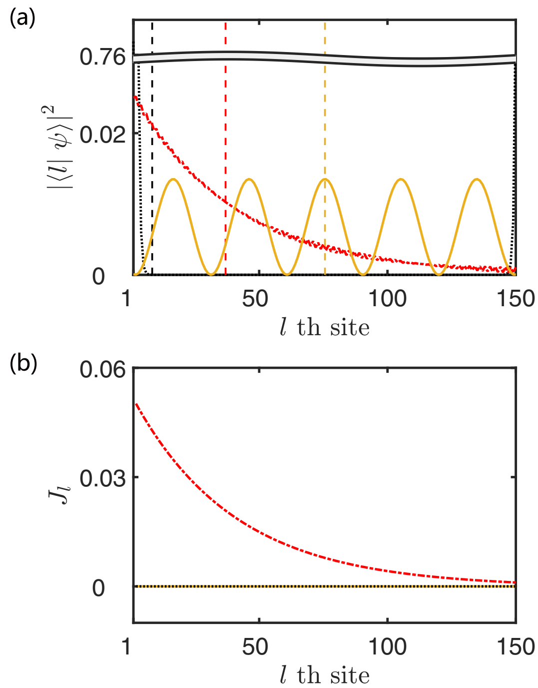

FIG. 4. Schematic illustrations for the concept of semilocalized state. (a) Plots of the profiles of three kinds of wave functions: localized state (the dotted black line), extended state (the solid yellow line), and semilocalized state (the dash-dotted red line). The decay length of the semilocalized state has the same order of the lattice length. The vertical dashed lines represent the value of center of mass for each state. We see that a semilocalized state is a crossover between localized and extended states. (b) Plots of the probability current distributions for three kinds of states. The currents for the extended state and local state are both zero. The current distribution of a semilocalized state exhibits a nonsteady behavior, violating the probability conservation, which is exclusive for the eigenstate of a non-Hermitian system. The size of the system is $N = 150$. Other parameters are $\nu = 5$, $\mu = 10$ for the dotted black lines, $\nu = 5$, $\mu = 0.1$ for dash-dotted red lines, and $\nu = 4$, $\mu = 2$ for the solid yellow lines.

a half-filled case where all the negative real parts of energy levels are filled by fermions. It is expected that the nonanalyticity of $g(\mu, \nu)$ can result in macroscopic phenomena.

First of all, we consider the density of ground-state energy, which is expressed as

$$E_g = \frac{2}{N}\sum_{n=1}^{N/2} \varepsilon_n = \frac{2}{N}\sum_{n=1}^{N/2} \mathrm{Re}(\varepsilon_n). \tag{19}$$

Here the term "ground state" is somehow controversial: (i) It takes only the real part of the energy into account but disregards the imaginary part. (ii) Although eigenenergy of the ground state is always real due to the conjugation-pair levels, the excited states may be unstable. Nevertheless, if the perturbation is restricted to conjugation-pair excitation, the ground state can be stable. In this context, we consider such a state as a ground state in this work. From the exact result in the Appendix, E_g is always analytical at all ranges of $\{\mu, \nu\}$, which seems to indicate that there is no occurrence of conventional QPT.

Second, we investigate the average CoM, which is defined as

$$R_{\mathrm{c}} = \frac{2}{N}\sum_{n=1}^{N/2} \langle r_{\mathrm{c}}\rangle_n. \tag{20}$$

From the exact result in the Appendix, we have

$$R_{\mathrm{c}} = \begin{cases} 1/2, & \mu, \nu > 1, \text{ or } \mu, \nu < 1 \\ 1/2 + \eta(\mu, \nu), & \text{otherwise} \end{cases}, \tag{21}$$

where $\eta(\mu, \nu)$ is a nonzero function. On the other hand, it is presumable that the nonanalyticity of $g(\mu, \nu)$ at $\mu\nu = 1$ can result in the nonanalyticity of R_{c}. Third, we investigate the average staggered current, which is defined as

$$\mathcal{J} = -\frac{2i}{N}\sum_{n=1}^{N/2}(-1)^n\left\langle \sum_{l=2}^{N}(c_l^\dagger c_{l+1} - \mathrm{H.c.})\right\rangle_n. \tag{22}$$

The feature of nonsteady eigenstates may also lead to nonanalyticity of $\mathcal{J}(\mu, \nu)$ at the nonanalytical point of $g(\mu, \nu)$.

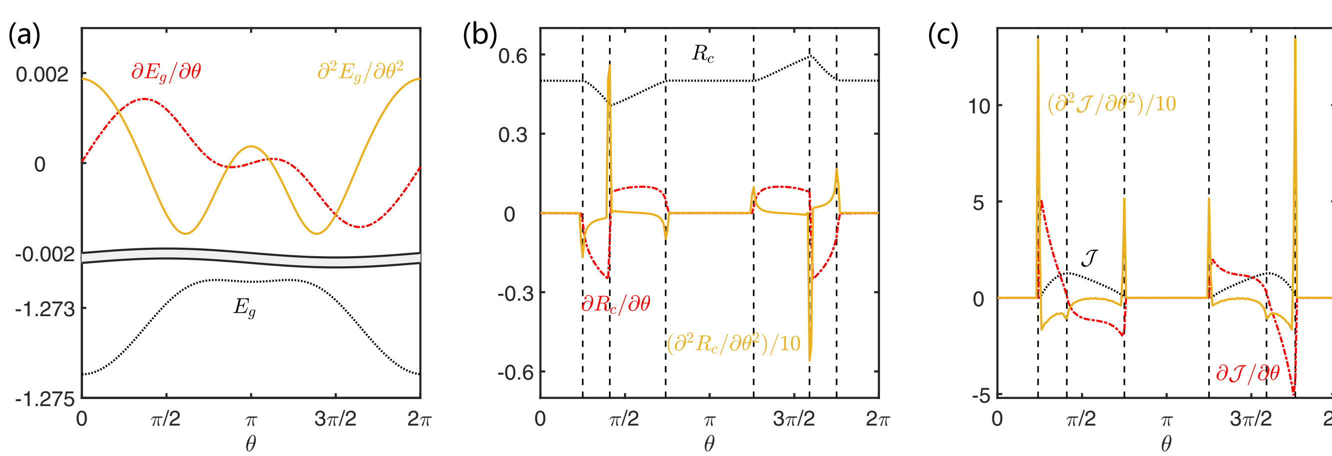

FIG. 5. Plots of three quantities (a) density of ground-state energy, (b) average CoM. (c) average staggered current, and the corresponding first-, second-order derivatives as a function of θ. This indicates that the density of the ground-state energy does not display any critical behaviors, while the other two exhibit the characteristics of second-order QPT; first-order derivatives are nonanalytical and second-order derivatives are divergent. The parameters are $\nu = 1 + 0.9\cos(\theta)$; $\mu = 1 + 0.9\sin(\theta)$. The size of the system is $N = 750$.

Actually we have

$$\mathcal{J} = \begin{cases} 0, & \mu, \nu \geqslant 1, \text{or } \mu, \nu \leqslant 1 \\ \neq 0, & \text{otherwise} \\ 4/\pi, & \mu\nu = 1 \end{cases}. \tag{23}$$

To demonstrate this point, we compute the quantities $\partial^n E_g/\partial\theta^n$, $\partial^n R_c/\partial\theta^n$, and $\partial^n \mathcal{J}/\partial\theta^n$ along the circle,

$$\nu = 1 + 0.9\cos(\theta), \quad \mu = 1 + 0.9\sin(\theta) \tag{24}$$

with $n = 1, 2$. In Fig. 5 we plot these quantities from exact diagonalization results for a finite-size system. We find that the density of ground-state energy does not display any critical behaviors as we predicted. It is different from a conventional QPT. It is understandable since the ground state does not experience a symmetry breaking as a whole, although a single-particle eigenstate has time-reversal symmetry breaking. However, the other two quantities exhibit the characteristics of second-order QPT: first-order derivatives are nonanalytical and second-order derivatives are divergent in the thermodynamic limit. Finally, we would like to stress that the QPT presented in this work is a many-particle effect. Then the behavior of the ratio $g(\mu, \nu)$ plays a crucial role to determine the phase diagram, which is a different topic from that in Ref. [79].

V. CONCLUSION

In summary, we have proposed a type of QPT beyond conventional symmetry-breaking and topological QPTs. It is based on the concept of a semilocalization state, which is a crossover from an extended to a localized state, possessing an exponential decay probability distribution. The peculiar feature is that the decay length is of the order of the size of the system, rather than fixed as a usual localized state. We have shown that such a semilocalized state can be induced by an asymmetrical dimer in a ring system. Remarkably, we found that a single dimer can result in a macroscopic amount of complex energy levels with semilocalized states, which determines the value of some macroscopic observables, such as the CoM and staggered current of the many-body ground state. Furthermore, the spectral statistics is nonanalytical as asymmetrical hopping strengths vary, resulting in a sudden charge of the ground state, i.e., QPT. Another distinguishing feature of such a QPT is the ground-state energy is analytical at the phase boundary. The symmetry of the many-body ground state remains unchanged, while the single-particle eigenstate breaks the time-reversal symmetry, resulting in the formation of a semilocalized state. It seems that such a quantum phase is exclusive for non-Hermitian systems.

ACKNOWLEDGMENTS

We acknowledge the support of the NSFC (Grant No. 11874225).

APPENDIX

In this Appendix, we present a detailed derivation and analysis for the Bethe ansatz solution of the Hamiltonian H.

1. Wave function

We consider the single-particle eigenstate

$$|\psi_n\rangle = \frac{1}{\sqrt{\Omega_n}} \sum_{l=1}^{N} f_n^l |l\rangle, \tag{A1}$$

following a Bethe ansatz form,

$$f_n^l = \begin{cases} 1, & l = 1 \\ A_n e^{ik_n l} + B_n e^{-ik_n l}, & l \in [2, N-1], \\ f_n^N & l = N \end{cases} \tag{A2}$$

where the normalization factor $\Omega_n = \sum_{n=1}^{N} |f_n^l|^2$ is determined by the Dirac inner product $\langle\psi_k|\psi_k\rangle = 1$. The Schrödinger equation

$$H|\psi_n\rangle = \varepsilon_n|\psi_n\rangle, \tag{A3}$$

with eigenenergy ε_n, can be expressed in explicit form as

$$f_n^{l-1} + f_n^{l+1} = \varepsilon_n f_n^l \tag{A4}$$

within the uniform region, and

$$\begin{aligned} f_n^3 + f_n^1 &= \varepsilon_n f_n^2 \\ f_n^2 + \nu f_n^N &= \varepsilon_n f_n^1 \\ f_n^{N-1} + \mu f_n^1 &= \varepsilon_n f_n^N \\ f_n^{N-2} + f_n^N &= \varepsilon_n f_n^{N-1} \end{aligned} \tag{A5}$$

around the asymmetric dimer. Substituting Eq. (A2) into Eqs. (A4) and (A5), we have

$$\varepsilon_n = 2\cos k_n \tag{A6}$$

and

$$\begin{aligned} A_n e^{ik_n} + B_n e^{-ik_n} &= f_n^1 \\ A_n e^{2ik_n} + B_n e^{-2ik_n} &= \varepsilon_n f_n^1 - \nu f_n^N \\ A_n e^{ik_n(N-1)} + B_n e^{-ik_n(N-1)} &= \varepsilon_n f_N - \mu f_1 \\ A_k e^{ik_n N} + B_k e^{-ik_n N} &= f_N, \end{aligned} \tag{A7}$$

and the solution of Eq. (A7) is

$$\begin{aligned} A_n &= \frac{1 - \nu e^{-ik_n} f_n^N}{2i\sin k_n} = \frac{\mu - e^{-ik_n} f_n^N}{2i\sin k_n e^{ik_n N}} \\ B_n &= \frac{\nu f_n^N e^{ik_n} - 1}{2i\sin k_n} = \frac{e^{ik_n} f_n^N - \mu}{2i\sin k_n e^{-ik_n N}}. \end{aligned} \tag{A8}$$

We would like to point out that the argument in the sine function can be a complex number. We note that $A_n = (B_n)^*$ if k_n is real, which indicates the reality of the wave function, $f_n^l = (f_n^l)^*$, obeying the time-reversal symmetry. The existence of a nontrivial solution (A_n, B_n) requires

$$(\mu + \nu)\sin k_n = \sin[k_n(1+N)] + \mu\nu\sin[k_n(1-N)]. \tag{A9}$$

And the solution of the wave function can be obtained from

$$\begin{aligned} A_n &= \frac{\nu - e^{ik_n N} - \nu e^{-2ik_n} + \mu\nu e^{ik_n(N-2)}}{2i\sin k_n(\nu - e^{ik_n N})} \\ B_n &= \frac{1 - \mu\nu}{2i\sin k_n(\nu e^{-ik_n N} - 1)} \end{aligned} \tag{A10}$$

and

$$f_n^N = \frac{e^{-ik_n} - \mu e^{ik_n(N-1)}}{\nu - e^{ik_n N}} f_1. \tag{A11}$$

In the following discussion, we use the normalized wave function

$$f_n^l = \sin(k_n l + \alpha_n),\ l \in [1, N] \tag{A12}$$

by replacing f_n^l by $\sqrt{\Omega_n} f_n^l$, where the coefficients are

$$\tan\alpha_n = \frac{c_n}{s_n}, \tag{A13}$$

$$\begin{aligned} s_n &= \nu^2 + 1 - \nu\cos(k_n N) + \nu\cos[k_n(N+2)] \\ &\quad - p_n \cos k_n, \\ c_n &= \nu\sin(k_n N) - \nu\sin[k_n(N+2)] + p_n \sin k_n, \end{aligned} \tag{A14}$$

with

$$\begin{aligned} p_n &= \cos[k_n(N+1)] - \mu\nu\cos[k_n(N-1)] \\ &\quad + (\mu+\nu)\cos k_n. \end{aligned} \tag{A15}$$

Similarly, the solution of $H^\dagger$ can be obtained as the form

$$\overline{f_n^l}(\mu,\nu) = \left[f_n^l(\nu,\mu)\right]^* \tag{A16}$$

and obey the biorthonormal relation

$$\sum_l \overline{f_m^l} f_n^l = \delta_{mn} \tag{A17}$$

if a biorthogonal inner product normalization factor is imposed.

Specifically, in the case with $\mu\nu = 1$ and $\mu > 1 > \nu$ (or $\mu < 1 < \nu$), Eq. (A9) reduces to

$$\sin[k_n(1+N)] + \sin[k_n(1-N)] - (\mu+\nu)\sin k_n = 0 \tag{A18}$$

and furthermore becomes

$$\cos(Nk_n) = \frac{\mu+\nu}{2}. \tag{A19}$$

Since $(\mu+\nu)/2 \geqslant 1$, we have

$$k_n = \frac{2n\pi}{N} + i\phi, \tag{A20}$$

where $\phi = (\ln\nu)/N$. Equation (A10) gives

$$\begin{aligned} A_k &= e^{-ik_n} \\ B_k &= 0, \end{aligned} \tag{A21}$$

so we have the wave function

$$f_l = e^{i\frac{2n\pi}{N}l} e^{-\phi l}, \qquad l \in [1, N] \tag{A22}$$

and the Dirac normalization factor

$$\Omega_n = \sum_{l=1}^{N} |f_l|^2 = \frac{1 - e^{-2\phi N}}{e^{2\phi} - 1}. \tag{A23}$$

2. Spectral statistics and phase diagram

Now we focus on the solution k_n of the transcendental equation, Eq. (A9). Without loss of generality, we have

$$k_n = \frac{2n\pi}{N} + \theta_n. \tag{A24}$$

For the general case ($n \neq N$ and $N/2$), Eq. (A9) becomes

$$\sin(\phi_n + \theta_n N) = \sin\Theta_n, \tag{A25}$$

where

$$\tan\phi_n = \frac{1+\mu\nu}{1-\mu\nu}\tan\frac{2n\pi}{N}, \tag{A26}$$

and we define

$$\Theta_n = \arcsin\frac{(\mu+\nu)\sin\frac{2n\pi}{N}}{\sqrt{(1+\mu^2\nu^2) - 2\mu\nu\cos\frac{4n\pi}{N}}}. \tag{A27}$$

We notice that ϕ_n is always real. Then the complex k_n arises from the complex θ_n, leading to

$$\left|\frac{(\mu+\nu)\sin\frac{2n\pi}{N}}{\sqrt{(1+\mu^2\nu^2) - 2\mu\nu\cos\frac{4n\pi}{N}}}\right| > 1, \tag{A28}$$

which is reduced to

$$\sin^2\frac{2n\pi}{N} > \frac{(\mu\nu-1)^2}{(\mu-\nu)^2}. \tag{A29}$$

We find that the most fragile energy level is $n = N/4$, so the complex energy levels start to appear if

$$(1-\nu)(1-\mu) < 0, \tag{A30}$$

which is the appearance condition of the complex levels. The most stable energy level is $n = 1$ or $N-1$, so all the $N-2$ energy levels turn to be complex at

$$\sin^2\frac{2\pi}{N} = \frac{(\mu\nu-1)^2}{(\mu-\nu)^2}. \tag{A31}$$

We define the proportion of the complex level as the ratio

$$g(\mu,\nu) = \frac{N_C(\mu,\nu)}{N}, \tag{A32}$$

where N_C is number of the complex levels. In the large-N limit, $\sin^2(2\pi/N) \to 0$, then we have

$$g(\mu,\nu) = \begin{cases} 0, & \mu,\nu \geqslant 1, \text{or } \mu,\nu \leqslant 1 \\ (\pi - 2k_c)/\pi, & \mu > 1 > \nu, \text{or } \mu < 1 < \nu, \\ 1, & \mu\nu = 1 \end{cases} \tag{A33}$$

with $k_c = |\arcsin[(1-\mu\nu)/(\nu-\mu)]|$. This expression clearly shows that $g(\mu,\nu)$ is nonanalytical at three curves $\mu = 1$, $\nu = 1$, and $\mu\nu = 1$.

At last, for $n = N$ or $N/2$, Eq. (A9) is reduced to

$$\tan\theta_N = \frac{(1-\mu\nu)\sin(\theta_N N)}{\mu+\nu-(1+\mu\nu)\cos(\theta_N N)}. \tag{A34}$$

θ_N is either real for some configuration of (μ,ν) or complex with $\mathrm{Re}\theta_N = \pi$ (0). For the second case, we take

$$\theta_N = \pi + i\epsilon \text{ or } i\epsilon, \tag{A35}$$

which corresponds to the real energy level but a localized state. The decay rate and energy can be obtained from ϵ, which obeys another transcending equation:

$$\tan(i\phi) = \frac{(\mu\nu - 1)\sin(Ni\epsilon)}{(1+\mu\nu)\cos(iN\epsilon) - (\mu+\nu)}. \tag{A36}$$

3. Energy levels

Next we will show that for a fixed n, Eq. (A25) must have a pair of solutions $(\theta_n, \overline{\theta}_n)$ leading to a pair of $(k_n, \overline{k}_n)$. We discuss this in the following cases.

(i) Real energy levels. In this case we have

$$\theta_n N = \Theta_n - \phi_n$$
$$\overline{\theta}_n N = \pi - \Theta_n - \phi_n, \tag{A37}$$

and accordingly,

$$k_n = \frac{2n\pi}{N} + \theta_n, \overline{k}_n = \frac{2n\pi}{N} + \overline{\theta}_n, \tag{A38}$$

for $n < N/2$. On the other hand, for the energy level $N-n$, we have

$$\tan\phi_{N-n} = -\frac{1+\mu\nu}{1-\mu\nu}\tan\frac{2n\pi}{N}, \tag{A39}$$

which means

$$\phi_{N-n} = 2\pi - \phi_n, \tag{A40}$$

in comparison with Eq. (A26). Furthermore, from

$$\sin(\phi_{N-n} + \theta_{N-n}N) = \sin\Theta_{N-n}, \tag{A41}$$

we get θ_{N-n} and $\overline{\theta}_{N-n}$ in the form of

$$\theta_{N-n}N = \pi - \Theta_{N-n} - \phi_{N-n} = -\overline{\theta}_n N$$
$$\overline{\theta}_{N-n}N = 2\pi + \Theta_{N-n} - \phi_{N-n} = -\theta_n N \tag{A42}$$

and

$$k_{N-n} = 2\pi - \overline{k}_n$$
$$\overline{k}_{N-n} = 2\pi - k_n. \tag{A43}$$

The corresponding energy levels satisfy $\varepsilon_{N-n} = \overline{\varepsilon}_n = 2\cos\overline{k}_n$ and $\overline{\varepsilon}_{N-n} = \varepsilon_n = 2\cos k_n$. In summary, if k_n $(n < \frac{N}{2})$ is real and

$$k_n = \frac{1}{N}[2n\pi + \Theta_n - \phi_n], \tag{A44}$$

with ε_n there must exist another

$$k_{n'} = \frac{1}{N}[(2n'+1)\pi - \Theta_{n'} - \phi_{n'}], \tag{A45}$$

with $n' = N - n$ and $\varepsilon_{n'} = \overline{\varepsilon}_n$. We see that k_n is a monotonic function except at the point $\mu = \nu = 1$. Thus the real energy levels are nondegenerate. The corresponding eigenstate has time-reversal symmetry since the wave function is real.

(ii) Complex energy levels. In this case, we have $\sin(\phi_n + \theta_n N) > 1$. The reality of $\sin(\phi_n + \theta_n N)$ requires that θ_n must be complex since ϕ_n is real. The two solutions of Eq. (A25) are

$$\theta_n N = \Theta_n - \phi_n$$
$$\overline{\theta}_n N = (\Theta_n)^* - \phi_n \tag{A46}$$

and, accordingly,

$$k_n = \frac{2n\pi}{N} + \theta_n$$
$$\overline{k}_n = \frac{2n\pi}{N} + \overline{\theta}_n, \tag{A47}$$

and the corresponding energy is $\varepsilon_n = 2\cos(2n\pi/N + \theta_n)$ and $\overline{\varepsilon}_n = 2\cos(2n\pi/N + \overline{\theta}_n)$. This indicates that

$$\overline{\varepsilon}_n = (\varepsilon_n)^*, \tag{A48}$$

i.e., the complex energy levels always come in pairs, and two energy levels coalesce when $\theta_n = \overline{\theta}_n$. On the other hand, for the energy level $N-n$, we have

$$\phi_{N-n} = 2\pi - \phi_n, \tag{A49}$$

which leads to

$$\theta_{N-n}N = \Theta_{N-n} - \phi_{N-n} = -\theta_n N - 2\pi$$
$$\overline{\theta}_{N-n}N = (\Theta_{N-n})^* - \phi_{N-n} = -\overline{\theta}_n N - 2\pi \tag{A50}$$

and

$$k_{N-n} = 2\pi - k_n - \frac{2\pi}{N}$$
$$\overline{k}_{N-n} = 2\pi - \overline{k}_n - \frac{2\pi}{N}. \tag{A51}$$

This indicates that the corresponding energy levels obey $\mathrm{Im}k_{N-n} = \mathrm{Im}k_n = -\mathrm{Im}\overline{k}_n$, $\varepsilon_{N-n} \approx \varepsilon_n$, $\overline{\varepsilon}_{N-n} \approx \overline{\varepsilon}_n$ for a large N limit.

In summary, if k_n $(n < \frac{N}{2})$ is complex and

$$k_n = \frac{1}{N}[2n\pi + \Theta_n - \phi_n], \tag{A52}$$

with ε_n there must exist another,

$$k_{n'} = \frac{1}{N}[2n'\pi + (\Theta_{n'})^* - \phi_{n'}], \tag{A53}$$

with $n' = N - n$ and $\varepsilon_{n'} = \overline{\varepsilon}_n$. We note that the corresponding eigenstate breaks time-reversal symmetry since the wave function is complex.

4. Center of mass

We still estimate the CoM in the following cases;

(i) Real energy levels. In this case, the eigenstate with real k_n has the form

$$|\psi_{\mathrm{R}}^n\rangle = \frac{1}{\sqrt{\Omega_n}}\sum_{l=1}^{N}\sin(k_n l + \alpha_n)|l\rangle, \tag{A54}$$

where

$$\alpha_n = \tan\frac{c_n}{s_n}$$

and $\Omega_n = \sum_{l=1}^{N}\sin^2(k_n l + \alpha_n)$ is the Dirac normalization factor. Then the CoM of the eigenstate $|\psi_{\mathrm{R}}^n\rangle$ is

$$\langle r_c^{\mathrm{R}}\rangle_n = \frac{1}{N}\sum_{l=1}^{N} l\langle\psi_{\mathrm{R}}^n|c_l^\dagger c_l|\psi_{\mathrm{R}}^n\rangle$$
$$= \frac{1}{N\Omega_n}\sum_{l=1}^{N} l\sin^2(lk_n + \alpha_n). \tag{A55}$$

Taking the approximation $k_n \approx 2n\pi/N$, together with the identities

$$\sum_{l=1}^{N} l \sin^2(lk_n + \alpha_n) \approx \frac{N^2}{4} - \frac{N \sin(k_n + 2\alpha_n)}{4 \sin k_n}$$
$$\sum_{l=1}^{N} \sin^2(lk_n + \alpha_n) \approx \frac{N}{2} - \frac{\cos((1+N)k_n + 2\alpha_n)}{2 \sin k_n \csc(k_n N)}, \tag{A56}$$

we have

$$\langle r_c^{\rm R} \rangle_n \approx \tfrac{1}{2}, \tag{A57}$$

which shows that all $|\psi_{\rm R}^n\rangle$ have the same CoM, located at the center of the lattice.

(ii) Complex energy levels. In this case, the eigenstates of the conjugate pair are expressed as

$$|\psi_+^n\rangle = \frac{1}{\sqrt{\Omega_n}} \sum_{l=1}^{N} \sin(k_n l + \alpha_n)|l\rangle, \tag{A58}$$

$$|\psi_-^n\rangle = \frac{1}{\sqrt{\Omega_n}} \sum_{l=1}^{N} \sin(k_n^* l + \alpha_n^*)|l\rangle. \tag{A59}$$

Similarly, the corresponding CoMs, defined as

$$\langle r_c^{\pm} \rangle_n = \frac{1}{N} \sum_{l=1}^{N} l \langle \psi_\pm | c_l^\dagger c_l | \psi_\pm \rangle, \tag{A60}$$

are identical with each other,

$$\langle r_c^+ \rangle_n = \langle r_c^- \rangle_n = \langle r_c \rangle_n, \tag{A61}$$

since $|\psi_+^n\rangle$ and $|\psi_-^n\rangle$ have the same distributions of Dirac probability. According to Eq. (A12), we have

$$\sum_{l=1}^{N} |\sin(k_n l + \alpha_n)|^2 \approx \frac{1}{2} \cosh(k_{\rm I} + k_{\rm I} N + 2\alpha_{\rm I}) {\rm csch}(k_{\rm I}) \sinh(k_{\rm I} N) \tag{A62}$$

and

$$\sum_{l=1}^{N} l |\sin(k_n l + \alpha_n)|^2 \approx \frac{1}{8} {\rm csch}^2 k_n^{\rm I} \big(\cosh 2\alpha_n^{\rm I} - (1+N) \cosh\big[2\big(k_n^{\rm I} N + \alpha_n^{\rm I}\big)\big] + N \cosh\big[2\big(k_n^{\rm I} + k_n^{\rm I} N + \alpha_n^{\rm I}\big)\big]\big), \tag{A63}$$

where

$$k_n^{\rm R} = {\rm Re} k_n,\ k_n^{\rm I} = {\rm Im} k_n,$$
$$\alpha_n^{\rm R} = {\rm Re}\alpha_n,\ \alpha_n^{\rm I} = {\rm Im}\alpha_n. \tag{A64}$$

Finally, we get

$$\langle r_c \rangle_n \approx \frac{N^{-1} \cosh\big(2\alpha_n^{\rm I}\big) - \cosh\big[2\big(k_n^{\rm I} N + \alpha_n^{\rm I}\big)\big] + \cosh\big[2\big(k_n^{\rm I} + k_n^{\rm I} N + \alpha_n^{\rm I}\big)\big]}{4 \cosh\big(k_n^{\rm I} + k_n^{\rm I} N + 2\alpha_n^{\rm I}\big) \sinh\big(k_n^{\rm I} N\big) \sinh\big(k_n^{\rm I}\big)}, \tag{A65}$$

which indicates that the CoM of the complex level has a distribution from 0 to 1.

For the special case with $\mu\nu = 1$, and $\mu > 1 > \nu$ (or $\mu < 1 < \nu$), it is readily obtained that

$$\langle r_c \rangle_n \approx \frac{1}{(\sqrt[N]{\nu^2} - 1)N} + \frac{1}{1 - \nu^2} \tag{A66}$$

in a large-N limit which is independent of n.

5. Current

We now turn to the current of eigenstate, which is defined as

$$J_l^n = -i\langle (c_l^\dagger c_{l+1} - {\rm H.c.}) \rangle_n$$
$$= -i\big(\big(f_n^l\big)^* f_n^{l+1} - \big(f_n^{l+1}\big)^* f_n^l\big). \tag{A67}$$

According to Eq. (A12), for the eigenstates with real k_n, we always have

$$J_l^n = 0. \tag{A68}$$

In contrast, for the eigenstates with complex k_n, we have

$$J_l^n = -i[\sin(k_n^* l + \alpha_n^*) \sin(k_n l + \alpha_n + k_n) - \sin(k_n^* l + k_n^* + \alpha_n^*) \sin(k_n l + \alpha_n)]. \tag{A69}$$

Taking a trigonometric transformation and an approximation $\sinh(k_n^{\rm I}) \approx 0$, one can obtain

$$J_l^n \approx -\sin\big(k_n^{\rm R}\big) \sinh\big(2k_n^{\rm I} l + 2\alpha_n^{\rm I} + k_n^{\rm I}\big).$$

We see that the current with k_n^* is $(J_l^n)^* = -J_l^n$, i.e., the sum current of a conjugate pair always vanishes. We introduce the concept of the average staggered current,

$$\mathcal{J} = -\frac{2i}{N} \sum_{n=1}^{N/2} (-1)^n \left\langle \sum_{l=2}^{N} (c_l^\dagger c_{l+1} - {\rm H.c.}) \right\rangle_n, \tag{A70}$$

which is nonzero for the band containing complex levels. A direct derivation yields

$$\left\langle \sum_{l=2}^{N} (c_l^\dagger c_{l+1} - {\rm H.c.}) \right\rangle_n = -i \sin\big(k_n^{\rm R}\big) {\rm csch}\big(k_n^{\rm I}\big) \sinh\big(k_n^{\rm I} N\big) \sinh\big(2k_n^{\rm I} + 2\alpha_n^{\rm I} + N k_n^{\rm I}\big) \tag{A71}$$

for large N. The average staggered current has the form

$$\mathcal{J} = -\frac{2}{N} \sum_{n=1}^{N/2} (-1)^n \sin\big(k_n^{\rm R}\big) {\rm csch}\big(k_n^{\rm I}\big) \times \sinh\big(k_n^{\rm I} N\big) \sinh\big(2k_n^{\rm I} + 2\alpha_n^{\rm I} + N k_n^{\rm I}\big). \tag{A72}$$

For the special case with $\mu\nu = 1$, in the large-N limit it is readily obtained that

$$\mathcal{J} \approx \frac{4}{\pi}. \tag{A73}$$

In summary, we have

$$\mathcal{J} = \begin{cases} 0, & \mu, \nu \geqslant 1, \text{or } \mu, \nu \leqslant 1 \\ \neq 0, & \text{otherwise} \\ 4/\pi, & \mu\nu = 1 \end{cases}, \tag{A74}$$

which has the implication that $\mathcal{J}$ can characterize the phase transitions.

[1] S. Sachdev, *Quantum Phase Transitions* (Cambridge University Press, Cambridge, England, 1999).

[2] X. L. Qi, Y. S. Wu, and S. C. Zhang, Topological quantization of the spin Hall effect in two-dimensional paramagnetic semiconductors, Phys. Rev. B **74**, 085308 (2006).

[3] M. Znojil, Conditional observability, Phys. Lett. B **650**, 440 (2007).

[4] M. Znojil, Tridiagonal PT-symmetric N-by-N Hamiltonians and a fine-tuning of their observability domains in the strongly non-Hermitian regime, J. Phys. A **40**, 13131 (2007).

[5] O. Bendix, R. Fleischmann, T. Kottos, and B. Shapiro, Exponentially Fragile $\mathcal{PT}$ Symmetry in Lattices with Localized Eigenmodes, Phys. Rev. Lett. **103**, 030402 (2009).

[6] S. Longhi, Bloch Oscillations in Complex Crystals with $\mathcal{PT}$ Symmetry, Phys. Rev. Lett. **103**, 123601 (2009).

[7] S. Longhi, Dynamic localization and transport in complex crystals, Phys. Rev. B **80**, 235102 (2009).

[8] L. Jin and Z. Song, Solutions of $\mathcal{PT}$ symmetric tight-binding chain and its equivalent Hermitian counterpart, Phys. Rev. A **80**, 052107 (2009).

[9] M. Znojil, Gegenbauer-solvable quantum chain model, Phys. Rev. A **82**, 052113 (2010).

[10] S. Longhi, Bloch oscillations in tight-binding lattices with defects, Phys. Rev. B **81**, 195118 (2010).

[11] S. Longhi, Periodic wave packet reconstruction in truncated tight-binding lattices, Phys. Rev. B **82**, 041106(R) (2010).

[12] L. Jin and Z. Song, Physics counterpart of the $\mathcal{PT}$ non-Hermitian tight-binding chain, Phys. Rev. A **81**, 032109 (2010).

[13] Y. N. Joglekar, D. Scott, M. Babbey, and A. Saxena, Robust and fragile $\mathcal{PT}$-symmetric phases in a tight-binding chain, Phys. Rev. A **82**, 030103(R) (2010).

[14] M. Znojil, An exactly solvable quantum-lattice model with a tunable degree of nonlocality, J. Phys. A **44**, 075302 (2011).

[15] M. Znojil, The crypto-Hermitian smeared-coordinate representation of wave functions, Phys. Lett. A **375**, 3176 (2011).

[16] H. Zhong, W. Hai, G. Lu, and Z. Li, Incoherent control in a non-Hermitian Bose-Hubbard dimer, Phys. Rev. A **84**, 013410 (2011).

[17] L. B. Drissi, E. H. Saidi, and M. Bousmina, Graphene, lattice field theory and symmetries, J. Math. Phys. **52**, 022306 (2011).

[18] Y. N. Joglekar and A. Saxena, Robust $\mathcal{PT}$ -symmetric chain and properties of its Hermitian counterpart, Phys. Rev. A **83**, 050101(R) (2011).

[19] D. D. Scott and Y. N. Joglekar, Degrees and signatures of broken $\mathcal{PT}$-symmetry in nonuniform lattices, Phys. Rev. A **83**, 050102(R) (2011).

[20] Y. N. Joglekar and J. L. Barnett, Origin of maximal symmetry breaking in even $\mathcal{PT}$-symmetric lattices, Phys. Rev. A **84**, 024103 (2011).

[21] D. D. Scott and Y. N. Joglekar, $\mathcal{PT}$-symmetry breaking and ubiquitous maximal chirality in a $\mathcal{PT}$-symmetric ring, Phys. Rev. A **85**, 062105 (2012).

[22] T. E. Lee and Y. N. Joglekar, $\mathcal{PT}$-symmetric Rabi model: Perturbation theory, Phys. Rev. A **92**, 042103 (2015).

[23] M. Kulishov *et al.*, Nonreciprocal waveguide Bragg gratings, Opt. Express **13**, 3068 (2005).

[24] S. Longhi, Transparency in Bragg scattering and phase conjugation, Opt. Lett. **35**, 3844 (2010).

[25] Z. Lin, H. Ramezani, T. Eichelkraut, T. Kottos, H. Cao, and D. N. Christodoulides, Unidirectional Invisibility Induced by $\mathcal{PT}$-Symmetric Periodic Structures, Phys. Rev. Lett. **106**, 213901 (2011).

[26] A. Regensburger, C. Bersch, M. Ali Miri, G. Onishchukov, D. N. Christodoulides, and U. Peschel, Parity-time synthetic photonic lattices, Nature (London) **488**, 167 (2012).

[27] T. Eichelkraut *et al.*, Mobility transition from ballistic to diffusive transport in non-Hermitian lattices, Nat. Commun. **4**, 2533 (2013).

[28] L. Feng, Y. L. Xu, W. S. Fegadolli, M. H. Lu, J. E. B. Oliveira, V. R. Almeida, Y. F. Chen, and A. Scherer, Experimental demonstration of a unidirectional reflectionless parity-time metamaterial at optical frequencies, Nat. Mater. **12**, 108 (2013).

[29] B. Peng, Ş. K. Özdemir, F. C. Lei, F. Monifi, M. Gianfreda, G. L. Long, S. H. Fan, F. Nori, C. M. Bender, and L. Yang, Parity–time-symmetric whispering-gallery microcavities, Nat. Phys. **10**, 394 (2014).

[30] L, Chang, X. S. Jiang, S. Y. Hua, C. Yang, J. M. Wen, L. Jiang, G. Y. Li, G. Z. Wang, and M. Xiao, Parity-time symmetry and variable optical isolation in active-passive-coupled microresonators, Nat. Photonics **8**, 524 (2014).

[31] S. Longhi, Invisibility in non-Hermitian tight-binding lattices, Phys. Rev. A **82**, 032111 (2010).

[32] S. Longhi and G. Della Valle, Invisible defects in complex crystals, Ann. Phys. (NY) **334**, 35 (2013).

[33] X. Z. Zhang and Z. Song, Momentum-independent reflectionless transmission in the non-Hermitian time-reversal symmetric system, Ann. Phys. (NY) **339**, 109 (2013).

[34] Y. Sun, W. Tan, H. Q. Li, J. Li, and H. Chen, Experimental Demonstration of a Coherent Perfect Absorber with $\mathcal{PT}$ Phase Transition, Phys. Rev. Lett. **112**, 143903 (2014).

[35] A. Mostafazadeh, Spectral Singularities of Complex Scattering Potentials and Infinite Reflection and Transmission Coefficients at Real Energies, Phys. Rev. Lett. **102**, 220402 (2009).

[36] S. Longhi, Spectral singularities in a non-Hermitian Friedrichs-Fano-Anderson model, Phys. Rev. B **80**, 165125 (2009).
[37] X. Z. Zhang, L. Jin, and Z. Song, Self-sustained emission in semi-infinite non-Hermitian systems at the exceptional point, Phys. Rev. A **87**, 042118 (2013).
[38] S. Longhi, Half-spectral unidirectional invisibility in non-Hermitian periodic optical structures, Opt. Lett. **40**, 5694 (2015).
[39] X. Q. Li, X. Z. Zhang, G. Zhang, and Z. Song, Asymmetric transmission through a flux-controlled non-Hermitian scattering center, Phys. Rev. A **91**, 032101 (2015).
[40] B. Peng, Ş. K. Özdemir, S. Rotter, H. Yilmaz, M. Liertzer, F. Monifi, C. M. Bender, F. Nori, and L. Yang, Loss-induced suppression and revival of lasing, Science **346**, 328 (2014).
[41] L. Feng, Z. J. Wong, R. M. Ma, Y. Wang, and X. Zhang, Single-mode laser by parity-time symmetry breaking, Science **346**, 972 (2014).
[42] H. Hodaei, M. A. Miri, M. Heinrich, D. N. Christodoulides, and M. Khajavikhan, Tunable parity-time-symmetric microring lasers, Science **346**, 975 (2014).
[43] L. Jin and Z. Song, Incident Direction Independent Wave Propagation and Unidirectional Lasing, Phys. Rev. Lett. **121**, 073901 (2018).
[44] C. Li, G. Zhang, X. Z. Zhang, and Z. Song, Conventional quantum phase transition driven by a complex parameter in a non-Hermitian PT-symmetric Ising model, Phys. Rev. A **90**, 012103 (2014).
[45] C. Li and Z. Song, Finite-temperature quantum criticality in a complex-parameter plane, Phys. Rev. A **92**, 062103 (2015).
[46] C. Li, G. Zhang, and Z. Song, Chern number in Ising models with spatially modulated real and complex fields, Phys. Rev. A **94**, 052113 (2016).
[47] C. Li, X. Z. Zhang, G. Zhang, and Z. Song, Topological phases in a Kitaev chain with imbalanced pairing, Phys. Rev. B **97**, 115436 (2018).
[48] R. Wang, X. Z. Zhang, Z. Song, Dynamical topological invariant for the non-Hermitian Rice-Mele model, Phys. Rev. A **98**, 042120 (2018).
[49] S. Lin, L. Jin, and Z. Song, Symmetry protected topological phases characterized by isolated exceptional points, Phys. Rev. B **99**, 165148 (2019).
[50] L. Jin and Z. Song, Bulk-boundary correspondence in a non-Hermitian system in one dimension with chiral inversion symmetry, Phys. Rev. B **99**, 081103(R) (2019).
[51] X. Z. Zhang and Z. Song, Partial topological Zak phase and dynamical confinement in a non-Hermitian bipartite system, Phys. Rev. A **99**, 012113 (2019).
[52] K. L. Zhang, H. C. Wu, L. Jin, and Z. Song, Topological phase transition independent of system non-Hermiticity, Phys. Rev. B **100**, 045141 (2019).
[53] B. B. Wei, S. W. Chen, H. C. Po, and R. B. Liu, Phase transitions in the complex plane of physical parameters, Sci. Rep. **4**, 5202 (2014).
[54] B. B. Wei and L. Jin, Universal critical behaviours in non-Hermitian phase transitions, Sci. Rep. **7**, 7165 (2017).
[55] T. E. Lee and C. K. Chan, Heralded Magnetism in Non-Hermitian Atomic Systems, Phys. Rev. X **4**, 041001 (2014).
[56] T. E. Lee, Anomalous Edge State in a Non-Hermitian Lattice, Phys. Rev. Lett. **116**, 133903 (2016).
[57] T. J. Elliott and I. B. Mekhov, Engineering many-body dynamics with quantum light potentials and measurements, Phys. Rev. A **94**, 013614 (2016).
[58] Y. Ashida, S. Furukawa, and M. Ueda, Quantum critical behavior influenced by measurement backaction in ultracold gases, Phys. Rev. A **94**, 053615 (2016),
[59] Y. Ashida, S. Furukawa, and M. Ueda, Parity-time-symmetric quantum critical phenomena, Nat. Commun. **8**, 15791 (2017).
[60] C. Korff and R. Weston, PT symmetry on the lattice: The quantum group invariant XXZ spin chain, J. Phys. A **40**, 8845 (2007).
[61] K. Kawabata, S. Higashikawa, Z. Gong, Y. Ashida, and M. Ueda, Topological unification of time-reversal and particle-hole symmetries in non-Hermitian physics, Nat. Commun. **10**, 297 (2019).
[62] S. Yao, F. Song, and Z. Wang, Non-Hermitian Chern Bands, Phys. Rev. Lett. **121**, 136802 (2018).
[63] Z. Gong, Y. Ashida, K. Kawabata, K. Takasan, S. Higashikawa, and M. Ueda, Topological Phases of Non-Hermitian Systems, Phys. Rev. X **8**, 031079 (2018).
[64] F. K. Kunst, E. Edvardsson, J. C. Budich, and E. J. Bergholtz, Biorthogonal Bulk-Boundary Correspondence in Non-Hermitian Systems, Phys. Rev. Lett **121**, 026808 (2018).
[65] T. M. Philip, M. R. Hirsbrunner, and M. J. Gilbert, Loss of Hall conductivity quantization in a non-Hermitian quantum anomalous Hall insulator, Phys. Rev. B **98**, 155430 (2018).
[66] D. Leykam, K. Y. Bliokh, C. L. Huang, Y. D. Chong, and F. Nori, Edge Modes, Degeneracies, and Topological Numbers in Non-Hermitian Systems, Phys. Rev. Lett. **118**, 040401 (2017).
[67] C. M. Bender, Making sense of non-Hermitian Hamiltonians, Rep. Prog. Phys. **70**, 947 (2007).
[68] Z. H. Musslimani, K. G. Makris, R. El-Ganainy, and D. N. Christodoulides, Optical Solitons in PT Periodic Potentials, Phys. Rev. Lett. **100**, 030402 (2008).
[69] K. G. Makris, R. El-Ganainy, D. N. Christodoulides, and Z. H. Musslimani, Beam Dynamics in PT Symmetric Optical Lattices, Phys. Rev. Lett. **100**, 103904 (2008).
[70] S. Klaiman, U. Günther, and N. Moiseyev, Visualization of Branch Points in PT-Symmetric Waveguides, Phys. Rev. Lett. **101**, 080402 (2008).
[71] C. E. Rüter, K. G. Makris, R. El-Ganainy, D. N. Christodoulides, Mordechai Segev, and D. Kip, Observation of parity-time symmetry in optics, Nat. Phys. **6**, 192 (2010).
[72] Y. D. Chong, L. Ge, H. Cao, and A. D. Stone, Coherent Perfect Absorbers: Time-Reversed Lasers, Phys. Rev. Lett. **105**, 053901 (2010).
[73] R. Fleury, D. Sounas, and A. Alù, An invisible acoustic sensor based on parity-time symmetry, Nat. Commun. **6**, 5905 (2015).
[74] N. Moiseyev, *Non-Hermitian Quantum Mechanics* (Cambridge University Press, Cambridge, UK, 2011).
[75] L. Feng, R. El-Ganainy, and L. Ge, Non-Hermitian photonics based on parity–time symmetry, Nat. Photon. **11**, 752 (2017).
[76] R. El-Ganainy, K. G. Makris, M. Khajavikhan, Z. H. Musslimani, S. Rotter, and D. N. Christodoulides, Non-Hermitian physics and PT symmetry, Nat. Phys. **14**, 11 (2018).
[77] S. K. Gupta, Y. Zou, X. Y. Zhu, M. H. Lu, L. Zhang, X. P. Liu, and Y. F. Chen, Parity-time symmetry in non-Hermitian complex media, arXiv:1803.00794.

[78] D. Christodoulides and J. Yang, *Parity-time Symmetry and Its Applications* (Springer, New York, 2018).
[79] P. Wang, Z. Song, and L. Jin, Non-Hermitian phase transition and eigenstate localization induced by asymmetric coupling, Phys. Rev. A **99**, 062112 (2019).
[80] C. Li, L. Jin, and Z. Song, Non-Hermitian interferometer: Unidirectional amplification without distortion, Phys. Rev. A **95**, 022125 (2017).
[81] S. Longhi, D. Gatti, and G. Della Valle, Robust light transport in non-Hermitian photonic lattices, Sci. Rep. **5**, 13376 (2015); Non-Hermitian transparency and one-way transport in low-dimensional lattices by an imaginary gauge field, Phys. Rev. B **92**, 094204 (2015).
[82] B. Midya, H. Zhao, and L. Feng, Non-Hermitian photonics promises exceptional topology of light, Nat. Commun. **9**, 2674 (2018).